MOLECULAR AND CELLULAR BIOLOGY, Nov. 2006, p. 8336–8346 Vol. 26, No. 22
0270-7306/06/$08.00+0 doi:10.1128/MCB.00425-06

Placental but Not Heart Defects Are Associated with Elevated Hypoxia-Inducible Factor α Levels in Mice Lacking Prolyl Hydroxylase Domain Protein 2▽†

Kotaro Takeda,[1] Vivienne C. Ho,[1] Hiromi Takeda,[1] Li-Juan Duan,[1] Andras Nagy,[2] and Guo-Hua Fong[1]*

Center for Vascular Biology, Department of Cell Biology, University of Connecticut Health Center, Farmington, Connecticut 06030,[1] and Samuel Lunenfeld Research Institute, Mount Sinai Hospital, 600 University Avenue, Toronto, Ontario, Canada M5G 1X5[2]

Received 10 March 2006/Returned for modification 21 April 2006/Accepted 27 August 2006

PHD1, PHD2, and PHD3 are *p*rolyl *h*ydroxylase *d*omain proteins that regulate the stability of hypoxia-inducible factor α subunits (HIF-α). To determine the roles of individual PHDs during mouse development, we disrupted all three *Phd* genes and found that *Phd2*$^{-/-}$ embryos died between embryonic days 12.5 and 14.5 whereas *Phd1*$^{-/-}$ or *Phd3*$^{-/-}$ mice were apparently normal. In *Phd2*$^{-/-}$ mice, severe placental and heart defects preceded embryonic death. Placental defects included significantly reduced labyrinthine branching morphogenesis, widespread penetration of the labyrinth by spongiotrophoblasts, and abnormal distribution of trophoblast giant cells. The expression of several trophoblast markers was also altered, including an increase in the spongiotrophoblast marker *Mash2* and decreases in the labyrinthine markers *Tfeb* and *Gcm1*. In the heart, trabeculae were poorly developed, the myocardium was remarkably thinner, and interventricular septum was incompletely formed. Surprisingly, while there were significant global increases in HIF-α protein levels in the placenta and the embryo proper, there was no specific HIF-α increase in the heart. Taken together, these data indicate that among all three PHD proteins, PHD2 is uniquely essential during mouse embryogenesis.

Hypoxia plays extremely important roles in physiological processes such as embryogenesis (15, 29). Hypoxia-inducible factors (HIFs) are essential players in cellular responses to hypoxia because they regulate the transcription of a large number of genes, including those encoding vascular endothelial growth factor A (VEGF-A) (8), erythropoietin (31), and glycolytic enzymes (32), which mediate cell adaptation to systemic and/or local hypoxic conditions. HIFs are heterodimeric transcription factors containing one of the three α-subunits (HIF-1α, HIF-2α, or HIF-3α) and a common β-subunit, which is also known as aryl hydrocarbon receptor nuclear translocator (18). While both α- and β-subunits are constitutively expressed at the transcriptional level, HIF-1α and HIF-2α protein levels fluctuate depending on oxygen tension; they are expressed at low levels under normoxia but significantly induced by hypoxia (30, 35, 36).

The stability of the HIF-1α and HIF-2α subunits is regulated by prolyl hydroxylase domain (PHD) proteins, which are members of the 2-oxoglutarate/iron dependent dioxygenase superfamily (4, 7). Hydroxylation at the 4 position of specific prolyl residues is responsible for the destabilization of HIF-1α and HIF-2α under normoxia (11, 13, 19). Hydroxylated HIF-α binds to von Hippel-Lindau protein (VHL) which targets it for polyubiquitination and proteasomal degradation (20). All of PHD1, PHD2, and PHD3 have K_m values for oxygen near normoxia (10), and their hydroxylase activities are suppressed under hypoxic conditions (7). Since mammalian cells in normal tissues are typically exposed to physiological hypoxia, it is curious how important different PHDs may be in vivo. Interestingly, a recent study demonstrated that a mutation in the human *Phd2* gene is a cause of erythrocytosis, a familial hereditary disease characterized by the production of excess numbers of erythrocytes (26). This finding demonstrates a critical role of PHD2 in normal human physiology.

In mice, several gene targeting studies have shown the essential roles of both HIF-1α (12, 29) and HIF-2α (25, 33) during embryonic development, but the roles of PHDs are not yet known. Since different PHDs have their own unique expression profiles (16), subcellular localization patterns (21), and specificities to HIF-1α and HIF-2α (2, 3), it is important to understand which PHD is critical for a specific biological process such as embryonic development.

In this paper we report that targeted disruption of the *Phd2* gene in mice led to significant increases in HIF-1α and HIF-2α expression and embryonic lethality between embryonic day 12.5 (E12.5) and E14.5. In contrast, mice homozygous for targeted disruptions in *Phd1* or *Phd3* genes are viable. These results suggest that PHD2 is a critical regulator of hypoxia response during embryonic development.

MATERIALS AND METHODS

Gene targeting of *Phd1*, *Phd2*, and *Phd3* loci. All three targeting constructs were designed similarly, and the *Phd2* targeting vector is described here (Fig. 1A). A 14-kb genomic DNA fragment spanning introns 1 to 4 was retrieved from a bacterial artificial chromosome clone (RP23-425M14; Invitrogen) into pL253 by recombination cloning (17). Next, exon 2 in the retrieved fragment was replaced with a cassette consisting of, in the following order, a 5′ recombination arm (644 bp to ~342 bp upstream of exon 2), a *loxP* site, exon 2 flanked by adjacent introns sequences (~230 bp on each side), a second *loxP* site, a neo-

* Corresponding author. Mailing address: Center for Vascular Biology, University of Connecticut Health Center, 263 Farmington Avenue, Farmington, CT 06030-3501. Phone: (860) 679-2373. Fax: (860) 679-1201. E-mail: fong@nso2.uchc.edu.

† Supplemental material for this article may be found at http://mcb.asm.org/.

▽ Published ahead of print on 11 September 2006.

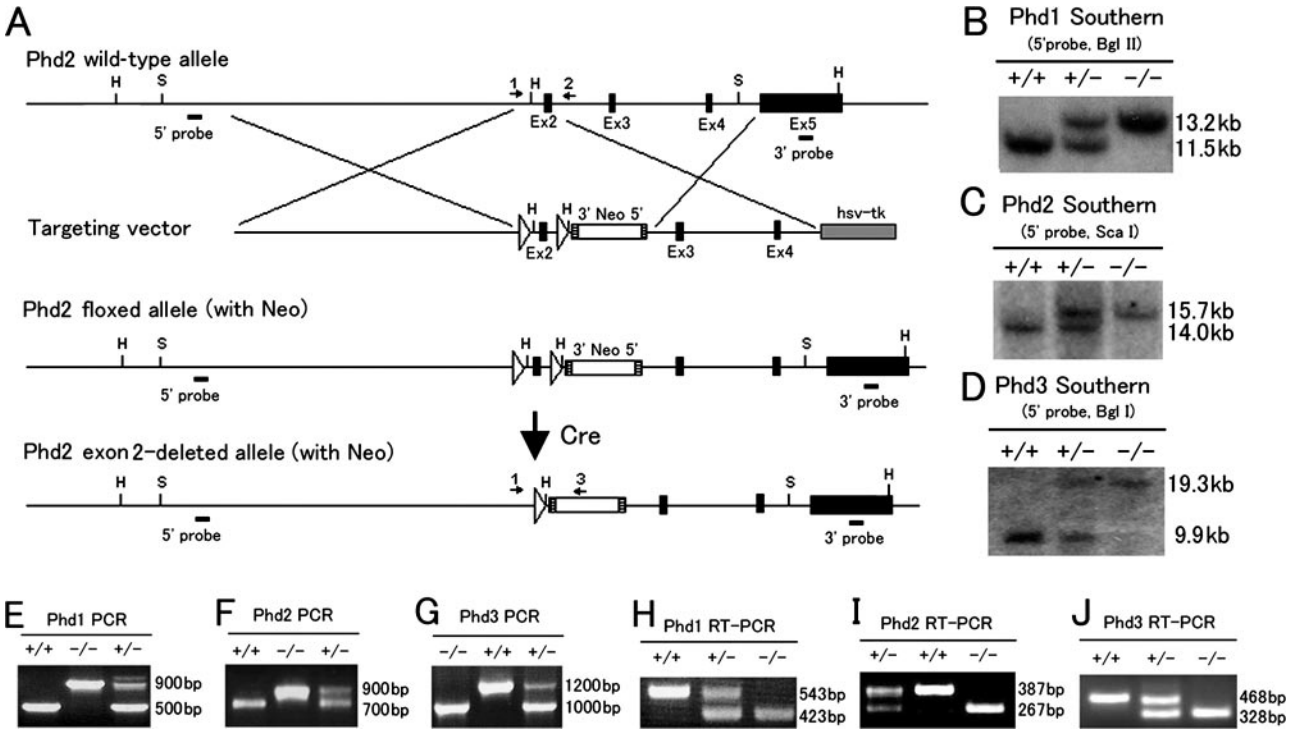

FIG. 1. Generation and analyses of targeted alleles for *Phd1*, *Phd2*, and *Phd3*. (A) Gene targeting strategy for *Phd2*. In targeted *Phd2* locus, exon 2 is flanked by two *loxP* sites. Exon 2 is deleted by Cre-mediated recombination. Ex, exon; hsv-tk, herpes simplex virus thymidine kinase; S, Sca I; H, Hind III; Neo, neomycin cassette; hatched square, *Frt* site (flanking the Neo cassette); open triangle, *loxP* site; arrows 1, 2 and 3, PCR primers for genotyping. (B to D) Southern blots for *Phd1*, *Phd2*, and *Phd3* loci demonstrating the deletion of floxed exons. (E to G) PCR of genomic DNA samples to confirm the deletion of floxed exons. Different relative sizes of the mutant and wild-type bands are due to the presence or absence of the neomycin cassette. (H to J) RT-PCR analyses to confirm the lack of wild-type mRNA transcripts in $Phd1^{-/-}$, $Phd2^{-/-}$, and $Phd3^{-/-}$ RNA samples.

mycin cassette (Neo) flanked by a pair of *Frt* sites, and a 3′ recombination arm (254 bp to ~506 bp 3′ to exon 2). Since *Phd1* has an untranslated exon 1, its exon 3 was targeted because it corresponded to exon 2 of *Phd2* and *Phd3*. For a description of the targeting vectors for *Phd1* and *Phd3*, see Fig. S1A and S1B in the supplemental material.

G4 hybrid embryonic stem (ES) cells of mixed C57BL/6 and 129/S6 background were used for gene targeting, and ES cell clones were screened by Southern blotting. Correctly targeted ES cells were used to generate viable mice by the tetraploid aggregation technique (22), and germ line transmission of the floxed alleles was achieved. After these mice were crossed with transgenic mice expressing Cre under the control of adenoviral EIIa promoter (EIIa Cre; stock no. 003314; Jackson Laboratory) (14), exon 2-deleted (for *Phd2* and *Phd3*) or exon 3-deleted (for *Phd1*) alleles were generated and are referred to as the "minus (−)" alleles for brevity. $Phd1^{+/-}$, $Phd2^{+/-}$, or $Phd3^{+/-}$ males were crossed with CD1 females for subsequent studies. In *Phd2* knockout mice, the neomycin cassette was deleted by crossing $Phd2^{+/-}$ mice with transgenic mice expressing Flpe under the control of β-actin promoter (Jackson Laboratory). The presence or absence of the cassette did not cause any difference in mutant phenotypes, and therefore distinctions are not made in data presentation. In *Phd3* knockout mice, the neomycin cassette was removed in targeted ES cells before generating mice. The neomycin cassette in $Phd1^{+/-}$ mice was never removed. All procedures used in handling mice were approved by the Animal Care Committee at the University of Connecticut Health Center in compliance with Animal Welfare Assurance.

Genotyping by Southern blotting and PCR. Information for Southern blotting (enzymes used, probes, and predicted fragment sizes) is summarized in Table S1 in the supplemental material. PCR primers used for genotyping are indicated as numbered arrows in relevant figures and are listed below: for *Phd1*, 5′-GGAG CTGGAGTTCTAGGTCAGGTT-3′ (arrow 1), 5′-TGAGACCAGGCAGAGG GAGTT-3′ (arrow 2), and 5′-AGGTGTCATTCTATTCTGGGGG-3′ (arrow 3) (see Fig. S1A in the supplemental material); for *Phd2*, 5′-AGGGCTTCTGGC ATTAGTTGACC-3′ (arrow 1), 5′-TTATCAACGTGACGGACATAGC-3′ (arrow 2), and 5′-AGGTGTCATTCTATTCTGGGGG-3′ (arrow 3) (Fig. 1A); for *Phd3*, 5′-CTCAGACCCCCTAAGTATGT-3′ (arrow 1) and 5′-CCACGTTAA CTCTAGAGCCACTGA-3′ (arrow 2) (see Fig. S1B in the supplemental material).

Northern blotting and PCR analysis. Total RNA samples were prepared using TRIzol reagent (Invitrogen) according to the manufacturer's protocol. RNA samples were separated on 1% denaturing agarose gels at 10 μg/lane, transferred to nylon membranes (Zeta-Probe GT Blotting Membrane; Bio-Rad, Hercules, CA), blocked by prehybridization, and hybridized with [^{32}P]dCTP-labeled cDNA probes. After a washing step, membranes were exposed to X-ray films (Kodak). cDNA probes are as follows (listed with nucleotide positions and associated GenBank accession numbers): *Vegfa*, nucleotides 383 to 629 (NM_009505); *Pgk1*, 423 to 649 (NM_008828); *Hif-1*α, 1467 to 1875 (NM_010431); and *Hif-2*α, 275 to 843 (NM_010137).

Total RNA was used for reverse transcription-PCR (RT-PCR) using a SuperScript One-Step RT-PCR kit (Invitrogen). The following primers were used: for *Phd1*, 5′-ACCGCGCAGCATTCGTG-3′ and 5′-GGGGCTGGCCATTAGGTA GGTGTA-3′; for *Phd2*, 5′-GCGGGAAGCTGGGCAACTAC-3′ and 5′-CAAC CCTCACACCTTTCTCACC-3′; for *Phd3*, 5′-CTGCGTGCTGGAGCGAGTC AA-3′ and 5′-TCATGTGGATTCCTGCGGTCTG-3′; for hypoxanthine phosphoribosyltransferase (*Hprt*), 5′-GCTGGTGAAAAGGACCTCT-3′ and 5′-CACAGGACTAGAACACCTGC-3′.

Quantitative real-time RT-PCR (Q-PCR) was performed using SYBR green PCR master mix (Applied Biosciences, Foster City, CA) and an ABI PRISM 7900HT Sequence Detection System. Expression data were presented as the mRNA relative level to that of *hprt* or glyceraldehyde-3-phosphate dehydrogenase (*Gapdh*). The following primers were used: for *vegha*, 5′-CACGACAGAA GGAGAGCAGAAGT-3′ and 5′-TTCGCTGGTAGACATCCATGAA-3′; for *hprt*, 5′-TCAGTCAACGGGGGACATAAA-3′ and 5′-GGGGCTGTACTGCT TAACCAG-3′; for *Tfeb*, 5′-CCACCCCAGCCATCAACAC-3′ and 5′-CAGAC AGATACTCCCGAACCTT-3′; for *Tpbp*, 5′-TTCCTAGTCATCCTATGCCTG G-3′ and 5′-GGTCATTTTCGCTACTGTGAAGT-3′; for placental lactogen 1

(*Pl1*), 5′-CAGGCTCCGGAATGCAATT-3′ and 5′-CCCAAAGGAATAGGCTTGACAC-3′; for *Mash2*, 5′-TGAAGGTGCAAACGTCCACTT-3′ and 5′-TACGAGTTCTGGTGCGGCA-3′; for *Gcm1*, 5′-GAGGAAGGCCGCAAGATTTA-3′ and 5′-GACAGCTTTTCCTCTGCTGCTT-3′; for *Phd1*, 5′-CATCAATGGGCGCACCA-3′ and 5′-GATTGTCAACATGCCTCACGTAC-3′; for *Phd2*, 5′-TAAACGGCCGAACGAAAGC-3′ and 5′-GGGTTATCAACGTGACGGACA-3′; for *Phd3*, 5′-CTATGTCAAGGAGCGGTCCAA-3′ and 5′-GTCCACATGGCGAACATAACC-3′.

Western blotting analysis and enzyme-linked immunosorbent assay (ELISA). For Western blotting, nuclear or total cell lysates were prepared. To prepare nuclear protein extracts, embryos were homogenized in a buffer containing 10 mM HEPES-KOH (pH 7.9), 1.5 mM $MgCl_2$, 10 mM KCl, 0.5 mM dithiothreitol, 0.2 mM phenylmethylsulfonyl fluoride, 0.2 mM deferoxamine, 0.1% NP-40, and 1× protease inhibitor cocktail (Complete; Roche Molecular Biochemicals). After centrifugation, pellets were resuspended at 0°C for 30 min in a buffer containing 20 mM HEPES-KOH (pH 7.9), 420 mM NaCl, 1.5 mM $MgCl_2$, 0.5 mM dithiothreitol, 0.2 mM deferoxamine, 1× protease inhibitor cocktail, 0.2 mM phenylmethylsulfonyl fluoride, and 25% glycerol. For total lysate extraction, tissues were lysed in radioimmunoprecipitation assay buffer (phosphate-buffered saline containing 1% Nonidet P-40, 0.5% sodium deoxycholate, 0.1% sodium dodecyl sulfate, and 1× protease inhibitor cocktail). The following antibodies were used: anti-HIF-1α and anti-HIF-2α (NB100-449 and NB100-122; Novus Biologicals); anti-HIF-3α (600-401-435; Rockland Immunochemicals); and anti-HIF-β (sc-5580; Santa Cruz Biotechnology). Anti-mouse PHD2 was custom-made (Maine Biotechnology Services) in Wistar rats against a C-terminal peptide (EKGVRVELKPNSVSKDV), and supernatants from fused hybridomas were used without clonal purification.

To quantify VEGF-A by ELISA, E11.5 hearts were sonicated in 100 μl of 250 mM Tris-HCl (pH 7.5) and cleared by centrifugation, and supernatants were subjected to ELISA using a Quantikine Mouse VEGF Immunoassay kit (MMV00; R&D Systems).

Histological analysis, immunohistochemistry, and RNA in situ hybridization. Embryos and placentas were fixed in 4% paraformaldehyde at 4°C overnight. For cryosections, fixed specimens were transferred to 30% sucrose overnight and embedded in OTC compound. For paraffin sections, specimens were dehydrated in ethanol and toluene before being embedded into paraffin. All sections were cut at 5 μm. Both cryosections and paraffin sections were stained with hematoxylin and eosin (HE) for general histological analysis. Cryosections were also subject to immunohistochemical (IHC) staining using anti-platelet endothelial cell adhesion molecule 1 (anti-PECAM-1) (MEC13.3; BD Pharmingen) and an ABC kit (Vector Laboratories).

RNA in situ hybridization was performed on paraffin sections using digoxigenin-labeled sense and antisense cDNA probes according to Wilkinson et al. (37), with the following modifications. Slides were prehybridized for 2 h with RNA hybridization buffer (50% formamide, 2× SSC [1× SSC is 0.15 M NaCl plus 0.015 M sodium citrate], 1× Denhardt's solution, 10% dextran sulfate, 0.5 mg/ml yeast tRNA, 0.5 mg/ml sonicated salmon sperm DNA) to reduce background and then hybridized with probes overnight at 65°C. Bound probes were detected with alkaline phosphatase-conjugated anti-digoxigenin antibody (Roche), and color was developed for 6 to 7 h with BCIP (5-bromo-4-chloro-3′-indolyphosphate) and Nitro-Blue Tetrazolium chloride (Promega). The following probes were used (with nucleotide positions and associated GenBank accession numbers): *Pl1*, nucleotides 145 to 583 (AF525161); and Tpbp, nucleotides 70 to 528 (NM_009411).

HE-stained paraffin sections were used for measurements of labyrinth thickness and giant cell counting. For each placenta, the average of three sections was used as one data point for statistical analysis. Giant cells were identified by their large cell bodies and nuclei (at least about three times the size of an average spongiotrophoblast) and their location near maternal tissues.

Whole-mount anti-PECAM-1 IHC of embryo and yolk sacs was performed as reported previously (25).

Statistical analysis. Statistical analyses were performed by a Student's *t* test. Data are shown as the mean ± standard error of the mean. A *P* value of <0.05 was considered to be statistically significant.

RESULTS

Generation of *Phd1*, *Phd2*, and *Phd3* knockout mice. Exon 2 in *Phd2* and *Phd3* or exon 3 in *Phd1* encodes sequences containing the essential His and Asp residues (His-271 and Asp-273 in PHD1, His-290 and Asp-292 in PHD2, and His-135 and Asp-137 in PHD3), which are required for Fe^{++} binding and hence prolyl hydroxylase activity (7). Therefore, we deleted exon 2 in *Phd2* and *Phd3* or exon 3 in *Phd1* by Cre-*loxP*-mediated recombination (Fig. 1A; see Fig. S1A for *Phd1* and S1B for *Phd3* in the supplemental material). Candidate ES cell clones were initially screened by Southern blotting, which identified multiple targeted clones for each locus (see Fig. S1C to H in the supplemental material). By crossing with EIIa Cre mice, exon 2- or exon 3-deleted alleles were generated. $Phd1^{+/-}$, $Phd2^{+/-}$, and $Phd3^{+/-}$ mice were viable and apparently normal. Further intercrosses between heterozygotes revealed that $Phd1^{-/-}$ and $Phd3^{-/-}$ mice were also viable. Southern blotting revealed that the deletion of floxed exons occurred correctly in $Phd1^{-/-}$ and $Phd3^{-/-}$ mice (Fig. 1B and D). The same conclusion was reached by PCR (Fig. 1E and G). Furthermore, RT-PCR demonstrated that in both $Phd1^{-/-}$ and $Phd3^{-/-}$ mice, no wild-type *Phd1* or *Phd3* mRNA was produced (Fig. 1H and J). Thus, we conclude that PHD1 and PHD3 are nonessential for viability in mice. In contrast, we did not find any $Phd2^{-/-}$ mice among 91 progenies after $Phd2^{+/-}$ intercrosses (Table 1), suggesting that PHD2 deficiency caused embryonic lethality.

TABLE 1. Genotypes of offspring from $Phd2^{+/-}$ intercrosses

Stage	No. of litters	No. of offspring with the indicated genotype			
		+/+ (alive)[a]	+/− (alive)[a]	−/− (alive)	−/− (dead)
E9.5	2	3	7	8	0
E10.5	7	18	30	15	0
E11.5	9	21	49	20	0
E12.5	5	16	26	13	0
E13.5	9	28	35	4	11
E14.5	2	2	6	0	4
E15.5	3	9	7	0	3
P21	17	32	59	0	0
Total	54	129	219	60	18

[a] There were no dead +/+ or +/− offspring.

Essential role of PHD2 in embryonic development. To investigate the development of $Phd2^{-/-}$ embryos, more than 300 embryos resulting from $Phd2^{+/-}$ intercrosses were dissected and examined between E9.5 and E15.5 (Table 1). Southern blotting (Fig. 1C) and PCR (Fig. 1F) revealed that $Phd2^{-/-}$ embryos were viable from E9.5 to E12.5, based on heart beating and overall morphology (Fig. 2A and B and Table 1). By RT-PCR, we also confirmed that no wild-type *Phd2* mRNA was present in $Phd2^{-/-}$ embryos (Fig. 1I), demonstrating the authenticity of gene disruption.

Embryonic lethality occurred after E12.5. At E13.5, approximately 70% of $Phd2^{-/-}$ embryos were dead, with their yolk sacs appearing pale (Fig. 2C to F and Table 1). Dead $Phd2^{-/-}$ embryos frequently displayed a dark redness around the heart and the abdominal region (Fig. 2F, arrowheads). After E14.5, no viable $Phd2^{-/-}$ embryos were found. These data demonstrate that $Phd2^{-/-}$ embryos die in utero between E12.5 and E14.5.

Since pale yolk sacs might be due to hemorrhage, we examined vascular development to determine if vascular defects might be responsible for embryonic lethality. By whole-mount

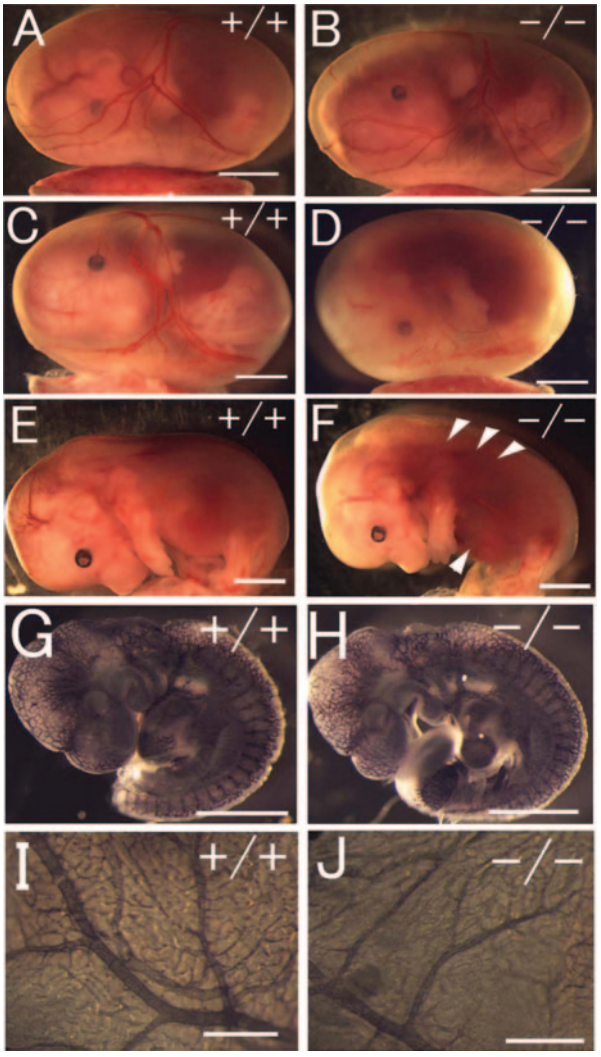

FIG. 2. Gross morphology of *Phd2*$^{-/-}$ embryos. (A and B) E12.5 *Phd2*$^{+/+}$ and *Phd2*$^{-/-}$ embryos with yolk sac. (C and D) E13.5 *Phd2*$^{+/+}$ and *Phd2*$^{-/-}$ embryos with yolk sac. (E and F) E13.5 *Phd2*$^{+/+}$ and *Phd2*$^{-/-}$ embryos after removal of yolk sacs. *Phd2*$^{-/-}$ embryos were alive at E12.5 and showed normal yolk sac vasculature. At E13.5, over 70% of *Phd2*$^{-/-}$ embryos were already dead, with a pale yolk sac. Arrowheads indicate dark-redness. (G to J) Whole-mount PECAM-1 immunohistochemistry. E9.5 *Phd2*$^{+/-}$ and *Phd2*$^{-/-}$ embryos (G and H). Images were captured by yolk sacs from E12.5 *Phd2*$^{+/-}$ and *Phd2*$^{-/-}$ embryos (I and J). Scale bars, 2 mm (A to F), 500 μm (G and H), 2 mm (I and J).

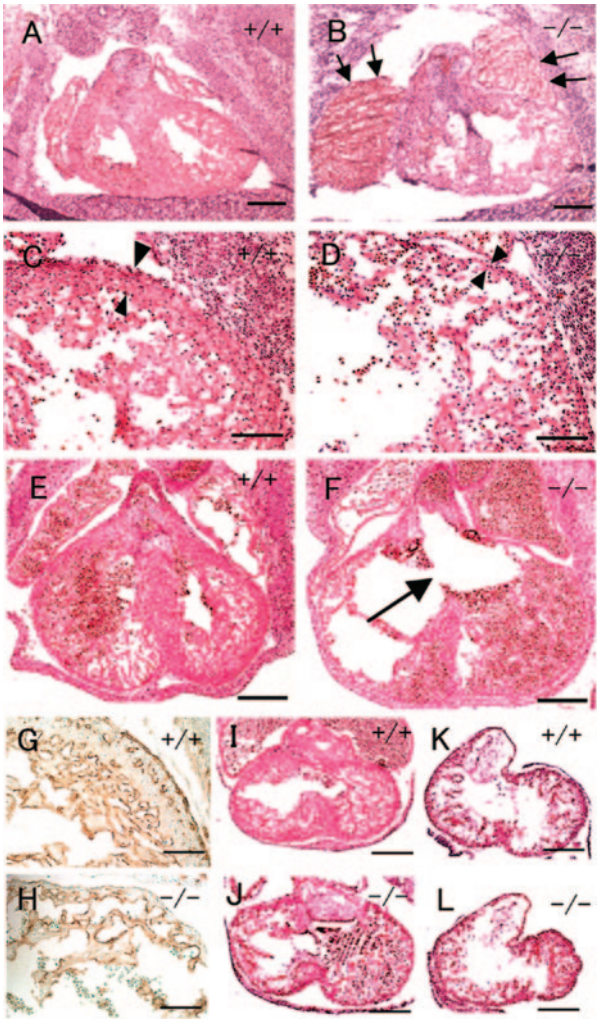

FIG. 3. Heart defects in *Phd2*$^{-/-}$ embryos. (A and B) HE-stained frontal heart sections of E12.5 embryos. Both right and left atria are enlarged and congested with fetal erythrocytes in *Phd2*$^{-/-}$ embryo (B, arrows). (C and D) Heart sections at a higher magnification. The ventricular wall (arrowheads) is much thinner in the *Phd2*$^{-/-}$ heart (D) than in the *Phd2*$^{+/+}$ control (C). Also, trabeculae appear underdeveloped in the *Phd2*$^{-/-}$ section. (E and F) HE-stained horizontal heart sections at E13.0. Note the disruption of the interventricular septum in the *Phd2*$^{-/-}$ embryo (F, arrow). (G and H) Anti-PECAM-1 IHC of E12.5 heart sections. (I and J) HE-stained heart sections at E11.5. The ventricular wall in the *Phd2*$^{-/-}$ heart is only slightly thinner than in the *Phd2*$^{+/+}$ control. (K and L) HE-stained heart sections at E10.5. Scale bars, 250 μm (A to F), 125 μm (G and H), and 250 μm (I to L).

anti-PECAM-1 IHC staining for embryos and yolk sacs from E9.5 through E12.5, we were unable to find significant defects (Fig. 2G to J). These results were in agreement with the grossly normal appearance of the vascular system in freshly dissected *Phd2*$^{-/-}$ embryos and yolk sacs at or before E12.5 (Fig. 2A and B). While these data do not exclude the possible existence of minor vascular defects, they indicate that there were no major vascular defects shortly before the occurrence of embryonic death at approximately E13.5. More likely, paleness in the yolk sac may be a secondary phenotype to embryonic death.

Severe cardiac defects in *Phd2*$^{-/-}$ embryos. Next, we examined heart development by histological analyses. At E12.5, heart development in *Phd2*$^{-/-}$ embryos was dramatically retarded. The compact layer of ventricles was much thinner than in normal littermates, the trabeculae were underdeveloped, and the intraventricular lumen was enlarged (Fig. 3A to D). By E13.0, the interventricular septum was completely closed in wild-type but not *Phd2*$^{-/-}$ embryos (Fig. 3E and F). We also evaluated the development of the endocardium by anti-PECAM-1 IHC staining. While the overall content of PECAM-1-positive cells was significantly reduced in *Phd2*$^{-/-}$ hearts, the remnant myocardial structures and trabeculae that did exist were well lined by PECAM-1-positive cells (Fig. 3G and H).

As expected, defective ventricular maturation resulted in cardiac failure in *Phd2*$^{-/-}$ embryos. Both atria were enlarged and congested with fetal erythrocytes (Fig. 3B, arrow), which was manifested as a dark red region in *Phd2*$^{-/-}$ embryos (Fig. 2F, arrowhead). In addition, jugular lymph sacs were dilated at E12.5 (data not shown).

To determine when cardiac defects first appeared in *Phd2*$^{-/-}$ embryos, heart development was examined at earlier stages. At E11.5, ventricular walls were slightly thinner in *Phd2*$^{-/-}$ embryos than in wild-type littermates (Fig. 3I and J), but the difference was much less obvious than at E12.5. At E10.5, *Phd2*$^{-/-}$ and wild-type hearts appeared very similar (Fig. 3K and L). Thus, we conclude that at the morphological level heart defect first occurred at approximately E11.5.

Significant defects in *Phd2*$^{-/-}$ placentas. An important step during placenta development is the extensive folding and branching of the chorionic ectoderm into the placenta and rapid growth of fetus-derived blood vessels from the chorion into these branched structures, forming a labyrinth of highly vascularized villi (28). Because of the high degree of vascularization, the labyrinth of wild-type placentas was bright red when viewed externally from the chorion side, and the edge of the labyrinth was clearly identified (Fig. 4A, arrowhead). But in *Phd2*$^{-/-}$ placentas, the edge was fuzzy, and patchy red spots were seen (Fig. 4B, arrow), suggesting that the labyrinth was irregularly formed. In histological sections, the maternal deciduum was normal, but the morphology of *Phd2*$^{-/-}$ placentas was grossly abnormal (Fig. 4C and D). In wild-type placentas, the labyrinths were densely packed with chorionic villi (also referred to as labyrinthine villi) (Fig. 4C). In contrast, in *Phd2*$^{-/-}$ placentas, the labyrinths contained sparse populations of villi, accompanied by large empty spaces (Fig. 4D). To confirm that the vast empty spaces were enlarged intervillous maternal lacunae rather than dilated blood vessels, anti-PECAM-1 IHC staining was performed (Fig. 4E and F). As shown in Fig. 4F, large spaces were not lined by PECAM-1-positive endothelial cells, indicating that they were intervillous spaces. Next, we determined when placental defects first occurred during development. As shown in Fig. 4G and H, enlarged intervillous spaces were abundant in *Phd2*$^{-/-}$ placentas at E11.5, but this phenotype was much less obvious at E10.5 (Fig. 4I and J). At E9.5, no morphological differences were found between wild-type and *Phd2*$^{-/-}$ placentas (Fig. 4K and L).

At E12.5, anti-PECAM-1 IHC staining also indicated reduced vascularization in *Phd2*$^{-/-}$ labyrinth (Fig. 4E and F). However, when labyrinthine villi were examined on an individual basis, vascularization of each *Phd2*$^{-/-}$ villous branch was similar to that of wild-type controls. Furthermore, before labyrinthine defects were obvious, there were no apparent vascular defects (data not shown). Thus, reduced vascularization did not appear to be an independent defect but was associated with reduced chorionic branching morphogenesis.

To further characterize placental defects, we evaluated several features of placenta development, including thickness of the labyrinth, number and distribution of giant cells, and morphogenesis of the spongiotrophoblast layer. At E11.5, we did not find statistically significant differences in labyrinth thickness (*Phd2*$^{+/+}$, 283 ± 18.7 μm; *Phd2*$^{+/-}$, 334 ± 11.0 μm; *Phd2*$^{-/-}$, 306 ± 30.2 μm; $n = 4$, $P > 0.05$ for all pairs of *t* tests).

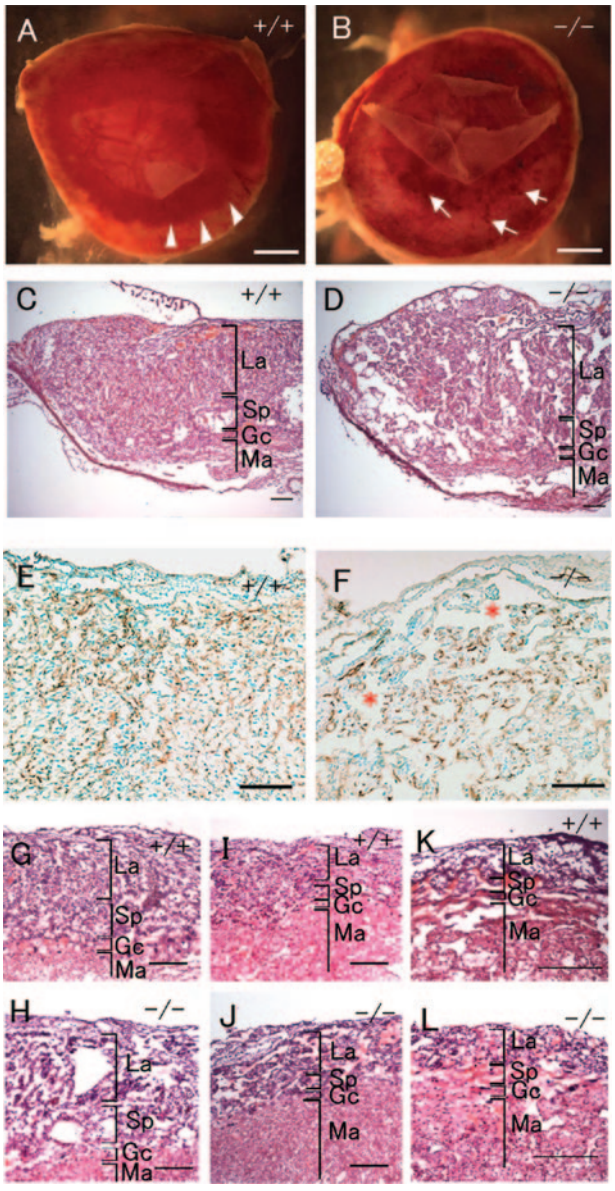

FIG. 4. Histological analysis of placental defects in *Phd2*$^{-/-}$ embryos. (A and B) External appearances of *Phd2*$^{+/+}$ and *Phd2*$^{-/-}$ placentas at E12.5. In the *Phd2*$^{+/+}$ placenta, the edge of the labyrinth can be identified clearly (A, arrowhead). In the *Phd2*$^{-/-}$ placenta, the edge is vague, and patchy red spots are present (B, arrow). (C and D) HE-stained placenta sections at E12.5. Large empty spaces are clearly visible in the labyrinth layer in the *Phd2*$^{-/-}$ (D) but not wild-type (C) placenta. (E and F) Anti-PECAM-1 IHC of *Phd2*$^{+/+}$ and *Phd2*$^{-/-}$ placentas at E12.5. Note that the large spaces (asterisks) are not lined with endothelial cells. (G to L) HE-stained placenta sections at E11.5 (G and H), E10.5 (I and J), and E9.5 (K and L). Morphological defects in the *Phd2*$^{-/-}$ placenta are apparent at E11.5 but much less obvious at E10.5. Sections from E9.5 placentas show no apparent difference between wild-type and *Phd2*$^{-/-}$ specimens. La, labyrinth; Sp, spongiotrophoblast zone; Gc, giant cells; Ma, maternal decidua. Scale bars, 1 mm (A and B), 250 μm (C and D), 125 μm (E and F), and 250 μm (G to L).

The total number of giant cells per section was not significantly different (*Phd2*$^{+/+}$, 52.0 ± 13.1; *Phd2*$^{+/-}$, 50.5 ± 9.1; and *Phd2*$^{-/-}$, 45.8 ± 6.8; $n = 4$, $P > 0.05$). However, near the center of the placenta (Fig. 5A to D), the number of giant

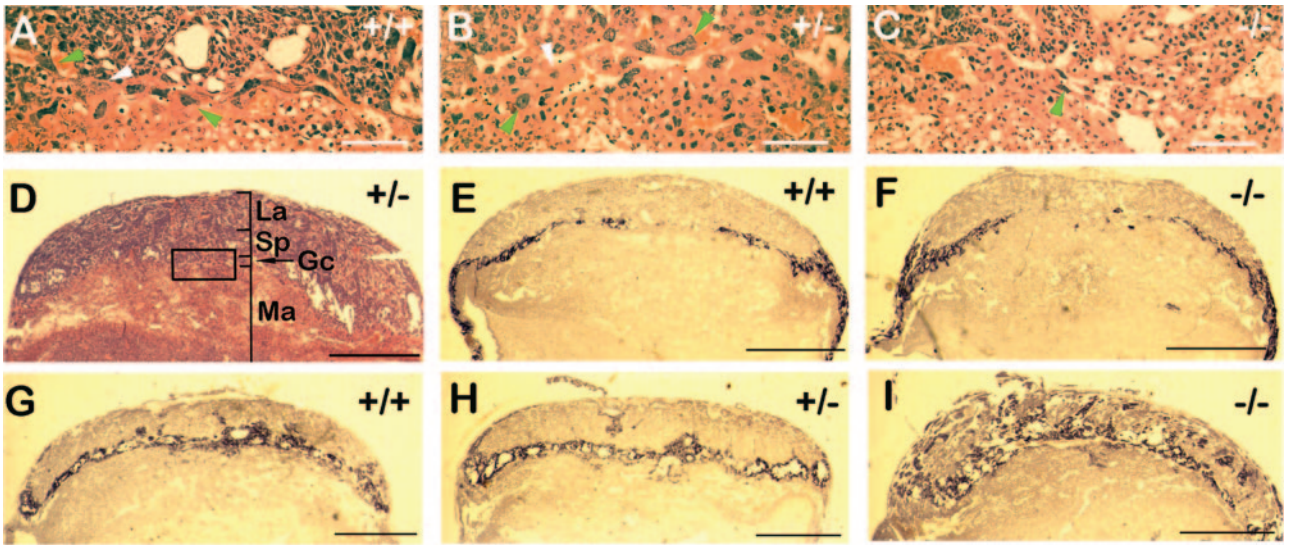

FIG. 5. Abnormal distributions of giant cells and spongiotrophoblasts in *Phd2*$^{-/-}$ placentas. (A to D) HE-stained placenta sections. The box in panel D indicates the position of the image in panel B. Images in panels A and C were taken from similar areas of *Phd2*$^{+/+}$ and *Phd2*$^{-/-}$ placenta sections. Green arrowheads in panels A and B indicate examples of giant cells with both large cell bodies and intensely stained large nuclei; white arrowheads indicate giant cells with large cell bodies but faint nuclei staining; the green arrowhead in panel C indicates giant cells in the central region of a *Phd2*$^{-/-}$ placenta. These "giant cells" are typically smaller than their counterparts in wild-type and *Phd2*$^{+/-}$ placentas, but their nuclei are still several times larger than nearby spongiotrophoblasts. Also, apparently reduced giant cell sizes were limited only to a small region near the center of the placenta, whereas the vast majority of giant cells did not appear to be different. (E to I) RNA in situ hybridization using *Pl1* (E and F) and *Tpbp* (G to I) antisense probes. Sense probes did not display background (not shown). The orientations of the images are the same as in panel D. Both E11.5 and E10.5 sections were used for *Pl1* hybridization; however, *Pl1* expression was difficult to detect at E11.5 due significant down-regulation in both normal and mutant placentas by this stage. Thus, only data for E10.5 sections are shown. For *Tpbp* hybridization, E11.5 sections were used. Note the presence of *Tpbp*$^{+}$ cells in the labyrinth layer of the *Phd2*$^{-/-}$ placenta. Scale bars, 100 μm (A to C) and 1 mm (D to I).

cells was significantly reduced in *Phd2*$^{-/-}$ mice (*Phd2*$^{+/+}$, 11.2 ± 1.6; *Phd2*$^{+/-}$, 11.0 ± 2.2; and *Phd2*$^{-/-}$, 4.2 ± 1.3; $n = 5$, $P < 0.05$ for t tests between +/+ and −/− or between +/− and −/−).

Placenta development was also evaluated by RNA in situ hybridizations for *Pl1* and *Tpbp*. At E10.5, distributions of *Pl1*$^{+}$ giant cells were only mildly different between wild-type and *Phd2*$^{-/-}$ placentas (Fig. 5E and F). Thus, it appeared that abnormal giant cell distribution first began at E10.5 and became apparent by E11.5. The distribution of spongiotrophoblasts was also grossly abnormal in *Phd2*$^{-/-}$ placentas by E11.5 (Fig. 5G to I). In wild-type and heterozygous placentas, the vast majority of spongiotrophoblasts existed as a layer of *Tpbp*$^{+}$ cells between the labyrinth and giant cells (Fig. 5G and H), with only occasional penetration of *Tpbp*$^{+}$ cells into the labyrinth. In *Phd2*$^{-/-}$ placentas, there was significant invasion of spongiotrophoblasts into the labyrinth (Fig. 5I).

Molecular analyses of *Phd2*$^{-/-}$ embryonic tissues. While embryonic lethality occurred between E12.5 to E14.5, the hypoxia pathway is likely defective at even earlier stages, leading to morphological manifestations by E12.5. To see if temporal regulation of PHD2 expression correlated with its functional requirement, we analyzed PHD2 protein levels at various stages of development. Western blotting revealed that PHD2 protein was present in wild-type embryos from E7.5 to E12.5 but significantly upregulated after E9.0 (Fig. 6A). As predicted, the ~45-kDa PHD2 protein was not found in *Phd2*$^{-/-}$ embryos (Fig. 6A). Unexpectedly, although a truncated PHD2 protein of 40 kDa was expected due to the deletion of exon 2-encoded sequence, this mutant protein could not be unequivocally detected by Western blotting. A weak band that might correspond to the truncated protein is indicated in Fig. 6A (arrow in right panel). The reason for the significant loss of the truncated protein is not clear, but probable causes may include posttranscriptional events such as reduced RNA and/or protein stability.

To confirm that developmental defects in *Phd2*$^{-/-}$ mice were due to the lack of PHD2 rather than to the possible presence of a trace amount of truncated form of the PHD2, we expressed *Phd2* cDNA in *Phd2*$^{-/-}$ embryos by an ES cell-based transgenic approach and confirmed that between E14.5 and 18.5, all eight *Phd2*$^{-/-}$ embryos expressing the transgene were viable, whereas all five nontransgenic littermates were dead (for more detailed description, see Fig S2 and Table S2 in the supplemental material). These data demonstrated that the absence of functional PHD2 was the cause of developmental defects in *Phd2*$^{-/-}$ mice.

To correlate expression of different *Phd* genes to developmental defects, we performed Q-PCR (Fig. 6B) and RT-PCR (Fig. 6C) for *Phd1*, *Phd2*, and *Phd3* mRNAs. In wild-type heart tissues of E11.5 embryos, *Phd2* mRNA was present at 3.9- and 7.8-fold of *Phd1* and *Phd3* mRNAs, respectively (Fig. 6B). Interestingly, the expression of *Phd3* mRNA was moderately upregulated in the heart of *Phd2*$^{-/-}$ mutants (Fig. 6C); however, both PHD1 and PHD3 proteins were below detectable levels by Western blotting (data not shown).

We also examined HIF expression from E9.5 to E11.5. HIF-1α levels in *Phd2*$^{-/-}$ embryos were dramatically increased

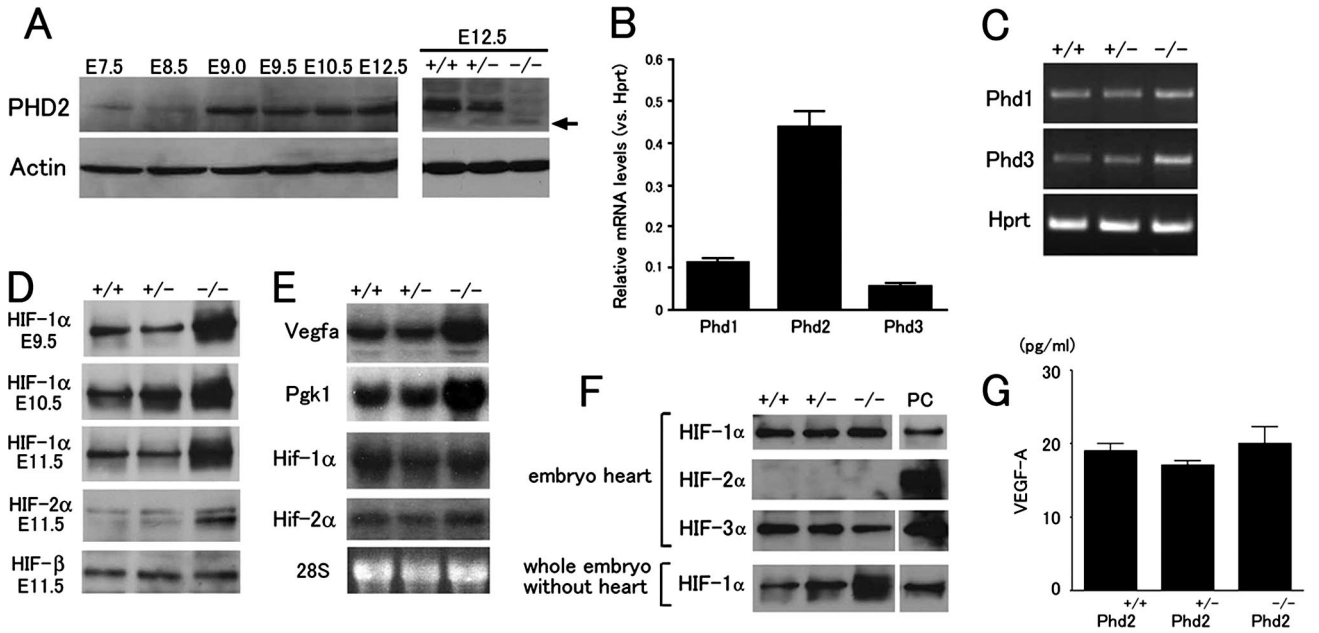

FIG. 6. Molecular analyses of *Phd2*$^{-/-}$ embryos. (A) Anti-PHD2 Western blot of total cell lysates from wild-type E7.5 to E12.5 embryos (left) or E12.5 embryos from *Phd2*$^{+/-}$ intercrosses (right). (B) Q-PCR for *Phd1*, *Phd2*, and *Phd3* using wild-type E11.5 hearts. Data are shown as relative abundances to *Hprt* mRNA level ($n = 6$). (C) RT-PCR for *Phd1* and *Phd3* using E11.5 hearts. *Hprt* was used as control. (D) Western blots of embryonic nuclear extracts. Developmental stages and antibodies used are indicated in the figure. (E) Northern blots of RNA prepared from whole embryos using cDNA probes specific for *Vegfa*, *Pgk1*, *Hif-1*α, and *Hif-2*α. (F) Western blots of E11.5 embryonic heart total extracts or nuclear extracts from the remaining tissues of embryo proper after removal of the heart. Antibodies are indicated in the figure. PC, positive controls, including nuclear extract of E11.5 wild-type embryo for HIF-1α, total extracts of E11.5 wild-type placenta for HIF-2α, and $CoCl_2$-treated NIH 3T3 cell total lysate for HIF-3α. (G) ELISA for VEGF-A in heart total lysates. Values are shown as means of protein concentration ($n = 4$). Genotypes in all panels refer to the *Phd2* locus.

over wild-type or *Phd2*$^{+/-}$ embryos at all stages examined (Fig. 6D). HIF-2α levels were also elevated in *Phd2*$^{-/-}$ embryos at E11.5, but HIF-β expression was unchanged (Fig. 6D). Since *Hif-1*α and *Hif-2*α mRNA levels were similar between wild-type and mutant embryos (Fig. 6E), elevated HIF-1α and HIF-2α protein levels in *Phd2*$^{-/-}$ embryos were most likely due to increased stability of these proteins. The expression of two important HIF target genes, *Vegfa* and phosphoglycerate kinase (*Pgk*) 1, was also upregulated in *Phd2*$^{-/-}$ embryos (Fig. 6E). These data demonstrate that PHD2 deficiency led to increased HIF-1α and HIF-2α protein levels, which were able to activate the transcription of their target genes.

To determine if HIF-α expression was also upregulated in the heart, we isolated hearts from E11.5 embryos and examined HIF-1α, HIF-2α, and HIF-3α protein levels by Western blotting. Unexpectedly, HIF-1α was not upregulated in *Phd2*$^{-/-}$ hearts, which was in sharp contrast to strong upregulation in the remainder of the embryo proper (Fig. 6F). HIF-2α expression was below detectable levels in both wild-type and mutant hearts, and the HIF-3α level was unchanged. We also determined the effect of PHD2 deficiency on *Vegfa* expression. While there was a 28% increase in *Vegfa* mRNA abundance according to Q-PCR (data not shown), VEGF-A protein level was essentially unchanged in the heart (Fig. 6G). These data suggested that the mechanisms regulating HIF-α and VEGF-A expression in the heart tissue may be complex and that the abundance of VEGF-A protein may be subject to multiple levels of controls.

Molecular analyses of *Phd2*$^{-/-}$ placental tissues. We also performed expression analysis for the placenta. Anti-PHD2 antibody detected a ~45-kDa protein in wild-type but not *Phd2*$^{-/-}$ placentas at E10.5 (Fig. 7A). Q-PCR using E10.5 wild-type placentas revealed that the *Phd2* mRNA level was present at 2.3- and 5.0-fold of *Phd1* and *Phd3*, respectively (Fig. 7B). RT-PCR revealed that *Phd3* but not *Phd1* expression appeared to be increased in *Phd2*$^{-/-}$ placentas (Fig. 7C), but neither PHD1 nor PHD3 proteins were detected by Western blotting (data not shown).

Both HIF-1α and HIF-2α protein levels were drastically increased in *Phd2*$^{-/-}$ placentas (Fig. 7D). Contrary to our expectation, however, both Q-PCR (Fig. 7E) and Northern blotting analyses (Fig. 7F) revealed that *Vegfa* mRNA levels remained similar between wild-type and *Phd2*$^{-/-}$ placentas. In addition, anti-VEGF-A IHC also failed to detect significant differences between wild-type and *Phd2*$^{-/-}$ placenta sections (data not shown). Taken together, these findings suggest that VEGF-A was unlikely to be a major candidate for placental defects.

Since histological analyses indicated abnormalities in all three major types of trophoblasts at E11.5, we wondered if expression of different trophoblast markers was already altered 1 day before morphological defects became clearly visible. Therefore, we isolated RNA samples from wild-type and *Phd2*$^{-/-}$ placentas at E10.5 and performed Q-PCR for transcriptional factor EB (*Tfeb*), *Gcm1*, *Mash2*, *Tpbp*, or *Pl1* (Fig. 7G). In *Phd2*$^{-/-}$ placentas, levels of syncytiotrophoblast mark-

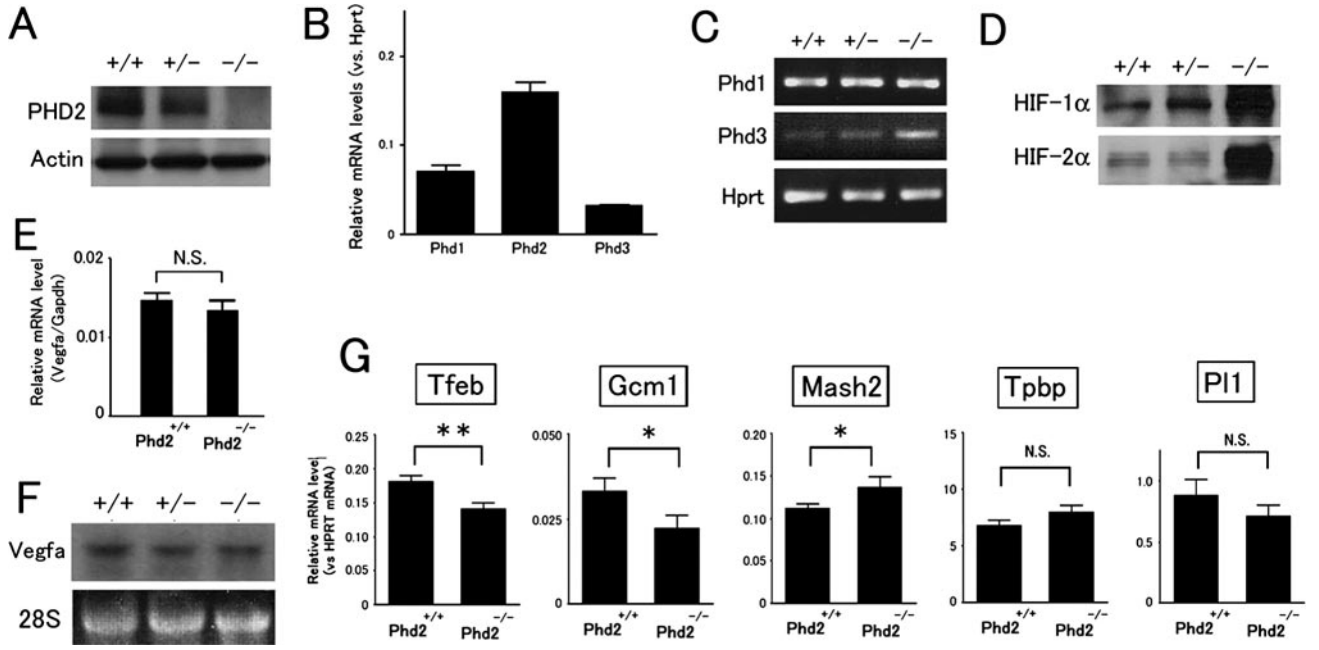

FIG. 7. Molecular analyses of *Phd2*$^{-/-}$ placentas. (A) Anti-PHD2 Western blot of cell lysates of E10.5 placentas. (B) Q-PCR for *Phd1*, *Phd2*, and *Phd3* mRNAs in wild-type E10.5 placentas. Values were normalized against *Hprt* level and are shown as means ± SEMs ($n = 6$). (C) *Phd1* and *Phd3* RT-PCR for E10.5 placentas. (D) Anti-HIF-1α and -HIF-2α Western blots of E10.5 placental cell extracts. (E) *Vegfa* Q-PCR for E10.5 placentas. Data are shown as means ± SEMs ($n = 4$). NS, not significant. (F) Northern blot of E10.5 placenta using *Vegfa* cDNA as a probe. (G) Q-PCR for trophoblast markers (indicated in the figure) in E10.5 placentas. **, $P < 0.01$; *, $P < 0.05$; NS, not significant ($n = 12$). Genotypes in all panels refer to the *Phd2* locus.

ers, *Tfeb* and *Gcm1*, were downregulated by 22.2% and 36.3%, respectively ($n = 12$, $P < 0.05$), and one of the spongiotrophoblast markers, *Mash2*, was upregulated by 22.5% ($n = 12$, $P < 0.05$). In addition, there were also trends of downregulation for the giant cell marker *Pl1* and upregulation of the spongiotrophoblast marker *Tpbp*, although these changes were statistically insignificant. Since these experiments were performed at a stage just before significant structural defects occurred, the resulting data are more likely to reflect primary changes of expression profiles rather than secondary changes due to structural abnormalities.

Normal placenta and cardiovascular development in *Phd1*$^{-/-}$ and *Phd3*$^{-/-}$ embryos. While *Phd1*$^{-/-}$ and *Phd3*$^{-/-}$ mice were viable, we examined whether there were any nonlethal developmental defects. We dissected embryos at E12.5 after intercrossing with *Phd*$^{+/-}$ or *Phd3*$^{+/-}$ mice and found that *Phd1*$^{-/-}$ or *Phd3*$^{-/-}$ embryos and yolk sacs appeared normal (Fig. 8A to D for *Phd1* and Fig. 9A to D for *Phd3*). At the molecular level, PHD2, HIF-1α, and HIF-2α protein levels and *Vegfa* and *Pgk1* mRNA levels were unchanged (data not shown). Lack of developmental defects was confirmed by histological analyses. In the heart, the thickness of ventricular walls and extent of trabeculation were similar between wild-type and *Phd1*$^{-/-}$ or *Phd3*$^{-/-}$ embryos (Fig. 8E to H for *Phd1* and Fig. 9E to H for *Phd3*). Anti-PECAM-1 IHC staining was performed to examine vascularity, but no abnormalities were found in either *Phd1*$^{-/-}$ or *Phd3*$^{-/-}$ embryos. Normal trabeculation and proper endocardial development were clearly visible in anti-PECAM-1-stained sections (Fig. 8I and J for *Phd1* and Fig. 9I and J for *Phd3*). The external appearances of *Phd1*$^{-/-}$ and *Phd3*$^{-/-}$ placentas were normal, and anti-PECAM-1 IHC staining in histological sections detected normal vascularization in the placenta (Fig. 8K and L for *Phd1*, Fig. 9K and L for *Phd3*, and data not shown). Finally, in histological sections, the overall structures of *Phd1*$^{-/-}$ and *Phd3*$^{-/-}$ placentas were indistinguishable from the wild type (Fig. 8M and N for *Phd1* and Fig. 9M and N for *Phd3*).

DISCUSSION

In this paper, we demonstrate that PHD2 is essential for normal mouse embryogenesis. *Phd2* knockout led to the upregulation of both HIF-1α and HIF-2α in the placenta as well as the embryo proper (except heart) prior to occurrence of embryonic lethality. Since normal embryos are known to be under physiological hypoxia (15, 29), our findings indicate that PHD2 is essential in the hypoxic environment during development. On the other hand, in vitro studies have shown that PHD2 is mainly functional under normoxia (2, 3) and that PHD2 activity is severely inhibited by hypoxia (6).

To explain this apparent controversy, we propose several models. In the first model, we suggest that the severity of hypoxia may vary both temporally and spatially during development and that PHD2 is functional when and where oxygen supply is adequate. For example, in hypoxic regions, HIF-1α and VEGF-A are colocalized (15) and may improve the local oxygen supply by inducing angiogenesis. After amelioration of hypoxia, PHD2 would become active and hydroxylate HIF-α, leading to the degradation of HIF-α subunits. In a second model, even in hypoxic regions, PHD2 may still be partially

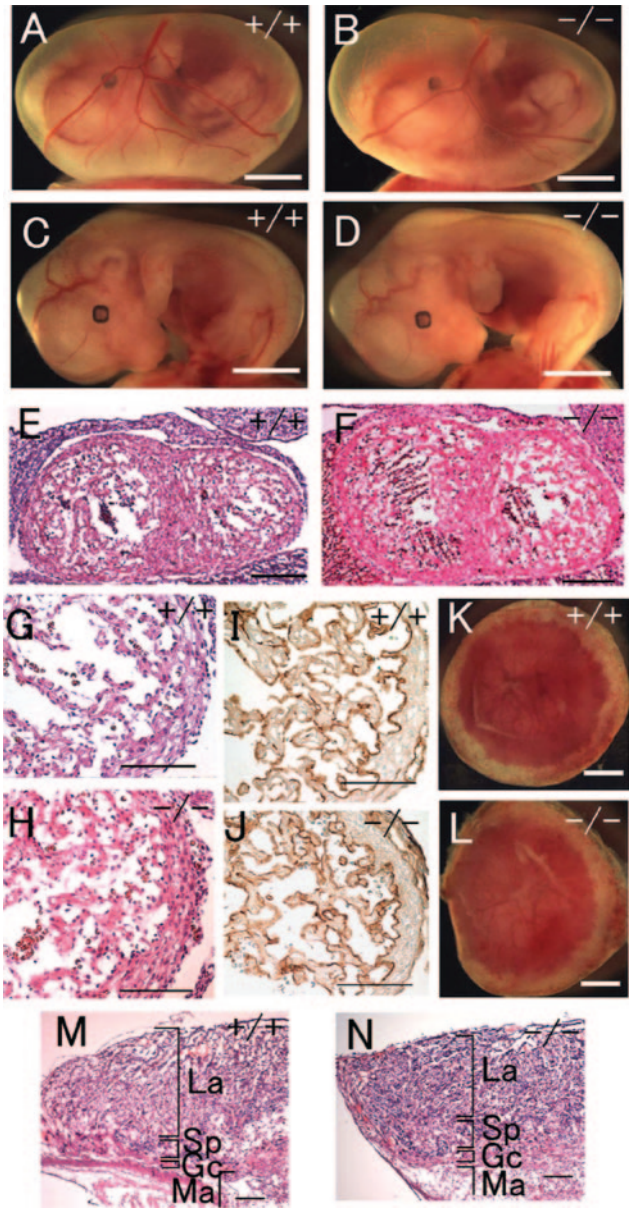

FIG. 8. Morphological analysis of *Phd1*$^{-/-}$ embryos and placentas at E12.5. (A and B) Embryos with yolk sacs. (C and D) Embryos after removal of yolk sacs. (E and F) HE-stained frontal heart sections. (G and H) Higher magnification of panels E and F. (I and J) Anti-PECAM-1 IHC staining of heart sections, showing similar ventricular wall thickness and trabeculae development in wild-type and *Phd1*$^{-/-}$ embryos. (K and L) External appearance of placentas. In both wild-type and *Phd1*$^{-/-}$ placentas, the labyrinth zones are nearly a uniform red and have well-defined boundaries. (M and N) HE-stained placenta sections. Scale bars, 2 mm (A to D), 250 μm (E and F), 125 μm (G to J), 1 mm (K and L), and 250 μm (M and N).

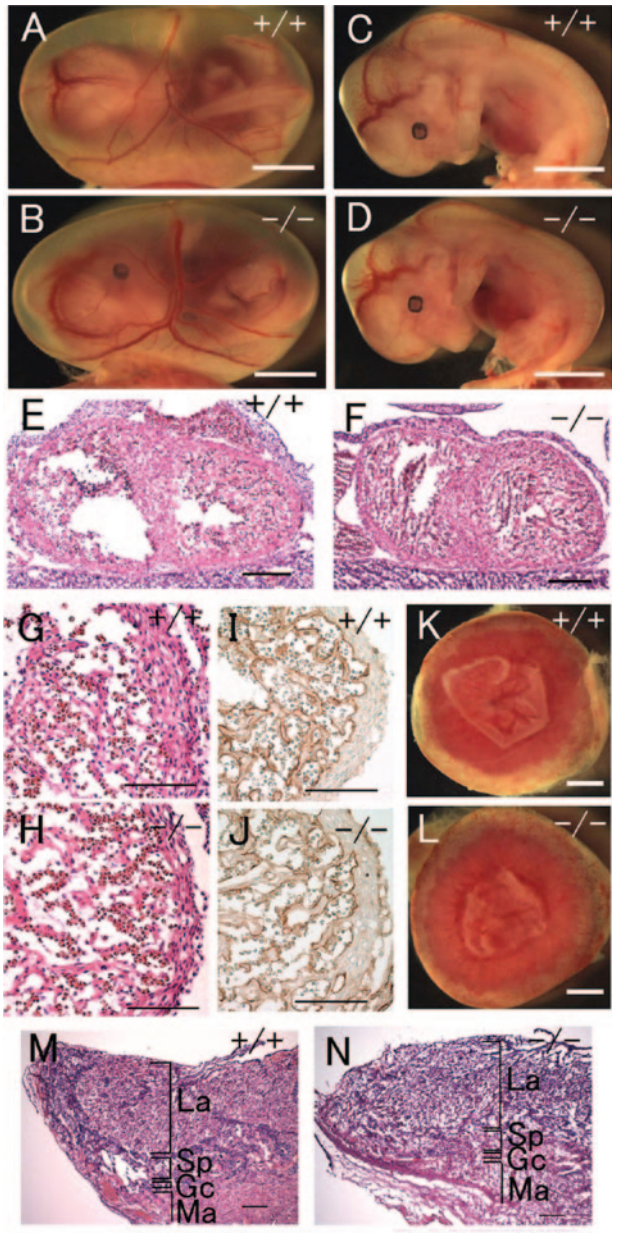

FIG. 9. Morphological analysis of *Phd3*$^{-/-}$ embryos and placentas at E12.5. (A and B) Embryos with yolk sacs. (C and D) Embryos after removal of yolk sacs. (E and F) HE-stained frontal heart sections. (G and H) Heart sections at higher magnifications. (I and J) Anti-PECAM-1 IHC staining of heart sections. (K to N) External appearances (K and L) and HE-stained sections of *Phd3*$^{+/+}$ and *Phd3*$^{-/-}$ placentas. No obvious differences can be found. Scale bars, 2 mm (A to D), 250 μm (E and F), 125 μm (G to J), 1 mm (K and L), and 250 μm (M and N).

active, and this residual hydroxylase activity may be essential for imposing limits on HIF-α expression. A third possibility is that PHD2 may have hydroxylase-independent functions, such as inhibition of HIF-1α transcriptional activity by direct binding interactions (24, 34). It should be emphasized that these models are not mutually exclusive but, rather, may work together in a cooperative manner.

The in vivo roles of PHD2 may likely involve more than HIF-α hydroxylation. This possibility is implied in the potentially complex causes of heart defects in *Phd2*$^{-/-}$ embryos. Contrary to our original expectation, there were no apparent increases in HIF-α levels in *Phd2*$^{-/-}$ hearts. Since HIF prolyl hydroxylases could also suppress HIF transcription activity by recruiting ING4 (24) or directly binding to HIF-α (34), future studies should address whether PHD2 deficiency in the heart

increases HIF-α transcriptional activity. Interestingly, a similar heart defect was not reported for *Vhl*$^{-/-}$ embryos (9). Although *Vhl*$^{-/-}$ embryos die earlier (E10.5 to E12.5) than *Phd2*$^{-/-}$ embryos, some *Vhl*$^{-/-}$ embryos did survive long enough (until E12.5) to allow the manifestation of heart defects if they were to occur as in *Phd2*$^{-/-}$ embryos. Different effects on heart development between PHD2 and VHL deficiencies raise the possibility that in addition to their common involvement in regulating HIF-α stability, PHD2 and VHL may have additional unique roles.

Lack of heart defects in *Vhl*$^{-/-}$ mice also indicates that poor placenta development does not necessarily cause heart defects prior to general deterioration of the embryo. This point is also supported by other examples where severe placental defects occurring at stages similar to their occurrence in *Phd2*$^{-/-}$ mice were not accompanied by heart defects (23, 27, 38). Thus, it is rather unlikely that the heart phenotype in *Phd2*$^{-/-}$ mice was a secondary defect due to placental insufficiency.

In contrast to the heart, *Phd2*$^{-/-}$ placentas displayed significantly increased HIF-α levels. Increased HIF-α expression in the placenta was associated with severe placental defects, including reduced villous branching morphogenesis in the labyrinth, altered distribution of spongiotrophoblasts, and giant cells. In spite of increased HIF-α expression, VEGF-A expression was unaltered in the placenta, and labyrinthine vascularization was reduced. However, while further studies are needed to determine if poor vascularization in the placenta is a primary defect, for a number of reasons we believe that it is more likely secondary to defective villous branching morphogenesis. First, we did not see an independent vascular defect prior to the onset of labyrinthine branching defects; second, in spite of an overall and apparent defect in vascular development in the labyrinth, villous branches that did exist were normally vascularized; third, villous branching morphogenesis is a known prerequisite for vascularization of the labyrinth (28) and, hence, insufficient villous development is expected to result in reduced vascularization in the placenta.

While both PHD2 and VHL are crucial for HIF-α degradation, *Phd2*$^{-/-}$ labyrinthine defects occurred approximately 1 day later and were less severe than in *Vhl*$^{-/-}$ placentas (9). For example, in *Vhl*$^{-/-}$ mice, development of syncytiotrophoblasts failed to occur, accompanied by lack of invasion of blood vessels into the placenta. In *Phd2*$^{-/-}$ placentas, syncytiotrophoblast differentiation did occur, although the expansion was reduced in the context of compromised villous branching morphogenesis. Also, fetal blood vessels invaded into *Phd2*$^{-/-}$ placentas, albeit with reduced efficiency, presumably due to poor villous branching. On the other hand, *Phd2*$^{-/-}$ placentas displayed spongiotrophoblast and giant cell abnormalities that were not reported for *Vhl*$^{-/-}$ mice. It is not clear what may be responsible for these differences, but several situations may be considered, including the possibility that VHL and PHD2 may have additional roles other than mediating HIF-α stability, possible compensations by other PHDs in *Phd2*$^{-/-}$ placentas, and likely differences in mouse strain backgrounds.

Some features of placental defects in *Phd2*$^{-/-}$ mice mirrored those in *Arnt*$^{-/-}$, *Hif-1*α$^{-/-}$, or *Hif-1*α$^{-/-}$ and *Hif-2*α$^{-/-}$ mice (1, 5). For example, *Mash2* expression decreased in *Hif-1*α$^{-/-}$ placentas, but it was increased in *Phd2*$^{-/-}$ placentas. While labyrinth phenotypes were not directly opposite between *Phd2*$^{-/-}$ and HIF-deficient mice, defects in *Phd2*$^{-/-}$ mice were in agreement with studies performed using trophoblast stem cells, which demonstrated that HIF deficiency promoted while hypoxia suppressed syncytiotrophoblast differentiation (1, 5).

In conclusion, our study demonstrates that PHD2 plays an essential role in the development of the heart and placenta. The fact that *Phd2*$^{-/-}$ but not *Phd1*$^{-/-}$ or *Phd3*$^{-/-}$ mice displayed severe placental and heart defects was consistent with our finding that *Phd2* was the most highly expressed *Phd* family member in these organs. On the other hand, our data do not exclude at least some partial functional compensation by PHD1 and PHD3. It remains to be determined if double or triple knockout mice would have more severe embryonic defects.

ACKNOWLEDGMENTS

This work was supported by U.S. Public Health grants 5P01HL70694. K.T. was partially supported by Uehara Memorial Foundation of Japan.

We are grateful to Neal Copeland for providing *Escherichia coli* strains and plasmid vectors for recombination cloning and to Nancy Ryan and Mitesh Shah for help.

REFERENCES

1. **Adelman, D. M., M. Gertsenstein, A. Nagy, M. C. Simon, and E. Maltepe.** 2000. Placental cell fates are regulated in vivo by HIF-mediated hypoxia responses. Genes Dev. **14:**3191–3203.
2. **Appelhoff, R. J., Y. M. Tian, R. R. Raval, H. Turley, A. L. Harris, C. W. Pugh, P. J. Ratcliffe, and J. M. Gleadle.** 2004. Differential function of the prolyl hydroxylases PHD1, PHD2, and PHD3 in the regulation of hypoxia-inducible factor. J. Biol. Chem. **279:**38458–38465.
3. **Berra, E., E. Benizri, A. Ginouves, V. Volmat, D. Roux, and J. Pouyssegur.** 2003. HIF prolyl-hydroxylase 2 is the key oxygen sensor setting low steady-state levels of HIF-1α in normoxia. EMBO J. **22:**4082–4090.
4. **Bruick, R. K., and S. L. McKnight.** 2001. A conserved family of prolyl-4-hydroxylases that modify HIF. Science **294:**1337–1340.
5. **Cowden Dahl, K. D., B. H. Fryer, F. A. Mack, V. Compernolle, E. Maltepe, D. M. Adelman, P. Carmeliet, and M. C. Simon.** 2005. Hypoxia-inducible factors 1α and 2α regulate trophoblast differentiation. Mol. Cell. Biol. **25:** 10479–10491.
6. **D'Angelo, G., E. Duplan, N. Boyer, P. Vigne, and C. Frelin.** 2003. Hypoxia up-regulates prolyl hydroxylase activity: a feedback mechanism that limits HIF-1 responses during reoxygenation. J. Biol. Chem. **278:**38183–38187.
7. **Epstein, A. C., J. M. Gleadle, L. A. McNeill, K. S. Hewitson, J. O'Rourke, D. R. Mole, M. Mukherji, E. Metzen, M. I. Wilson, A. Dhanda, Y. M. Tian, N. Masson, D. L. Hamilton, P. Jaakkola, R. Barstead, J. Hodgkin, P. H. Maxwell, C. W. Pugh, C. J. Schofield, and P. J. Ratcliffe.** 2001. *C. elegans* EGL-9 and mammalian homologs define a family of dioxygenases that regulate HIF by prolyl hydroxylation. Cell **107:**43–54.
8. **Forsythe, J. A., B. H. Jiang, N. V. Iyer, F. Agani, S. W. Leung, R. D. Koos, and G. L. Semenza.** 1996. Activation of vascular endothelial growth factor gene transcription by hypoxia-inducible factor 1. Mol. Cell. Biol. **16:**4604–4613.
9. **Gnarra, J. R., J. M. Ward, F. D. Porter, J. R. Wagner, D. E. Devor, A. Grinberg, M. R. Emmert-Buck, H. Westphal, R. D. Klausner, and W. M. Linehan.** 1997. Defective placental vasculogenesis causes embryonic lethality in VHL-deficient mice. Proc. Natl. Acad. Sci. USA **94:**9102–9107.
10. **Hirsila, M., P. Koivunen, V. Gunzler, K. I. Kivirikko, and J. Myllyharju.** 2003. Characterization of the human prolyl 4-hydroxylases that modify the hypoxia-inducible factor. J. Biol. Chem. **278:**30772–30780.
11. **Ivan, M., K. Kondo, H. Yang, W. Kim, J. Valiando, M. Ohh, A. Salic, J. M. Asara, W. S. Lane, and W. G. Kaelin, Jr.** 2001. HIFα targeted for VHL-mediated destruction by proline hydroxylation: implications for O2 sensing. Science **292:**464–468.
12. **Iyer, N. V., L. E. Kotch, F. Agani, S. W. Leung, E. Laughner, R. H. Wenger, M. Gassmann, J. D. Gearhart, A. M. Lawler, A. Y. Yu, and G. L. Semenza.** 1998. Cellular and developmental control of O2 homeostasis by hypoxia-inducible factor 1α. Genes Dev. **12:**149–162.
13. **Jaakkola, P., D. R. Mole, Y. M. Tian, M. I. Wilson, J. Gielbert, S. J. Gaskell, A. Kriegsheim, H. F. Hebestreit, M. Mukherji, C. J. Schofield, P. H. Maxwell, C. W. Pugh, and P. J. Ratcliffe.** 2001. Targeting of HIF-alpha to the von Hippel-Lindau ubiquitylation complex by O2-regulated prolyl hydroxylation. Science **292:**468–472.

14. **Lakso, M., J. G. Pichel, J. R. Gorman, B. Sauer, Y. Okamoto, E. Lee, F. W. Alt, and H. Westphal.** 1996. Efficient in vivo manipulation of mouse genomic sequences at the zygote stage. Proc. Natl. Acad. Sci. USA **93:**5860–5865.
15. **Lee, Y. M., C. H. Jeong, S. Y. Koo, M. J. Son, H. S. Song, S. K. Bae, J. A. Raleigh, H. Y. Chung, M. A. Yoo, and K. W. Kim.** 2001. Determination of hypoxic region by hypoxia marker in developing mouse embryos in vivo: a possible signal for vessel development. Dev. Dyn. **220:**175–186.
16. **Lieb, M. E., K. Menzies, M. C. Moschella, R. Ni, and M. B. Taubman.** 2002. Mammalian EGLN genes have distinct patterns of mRNA expression and regulation. Biochem. Cell Biol. **80:**421–426.
17. **Liu, P., N. A. Jenkins, and N. G. Copeland.** 2003. A highly efficient recombineering-based method for generating conditional knockout mutations. Genome Res. **13:**476–484.
18. **Maltepe, E., J. V. Schmidt, D. Baunoch, C. A. Bradfield, and M. C. Simon.** 1997. Abnormal angiogenesis and responses to glucose and oxygen deprivation in mice lacking the protein ARNT. Nature **386:**403–407.
19. **Masson, N., and P. J. Ratcliffe.** 2003. HIF prolyl and asparaginyl hydroxylases in the biological response to intracellular O(2) levels. J. Cell Sci. **116:**3041–3049.
20. **Maxwell, P. H., M. S. Wiesener, G. W. Chang, S. C. Clifford, E. C. Vaux, M. E. Cockman, C. C. Wykoff, C. W. Pugh, E. R. Maher, and P. J. Ratcliffe.** 1999. The tumour suppressor protein VHL targets hypoxia-inducible factors for oxygen-dependent proteolysis. Nature **399:**271–275.
21. **Metzen, E., U. Berchner-Pfannschmidt, P. Stengel, J. H. Marxsen, I. Stolze, M. Klinger, W. Q. Huang, C. Wotzlaw, T. Hellwig-Burgel, W. Jelkmann, H. Acker, and J. Fandrey.** 2003. Intracellular localisation of human HIF-1 α hydroxylases: implications for oxygen sensing. J. Cell Sci. **116:**1319–1326.
22. **Nagy, A., J. Rossant, R. Nagy, W. Abramow-Newerly, and J. C. Roder.** 1993. Derivation of completely cell culture-derived mice from early-passage embryonic stem cells. Proc. Natl. Acad. Sci. USA **90:**8424–8428.
23. **Nakamura, Y., Y. Hamada, T. Fujiwara, H. Enomoto, T. Hiroe, S. Tanaka, M. Nose, M. Nakahara, N. Yoshida, T. Takenawa, and K. Fukami.** 2005. Phospholipase C-δ1 and -δ3 are essential in the trophoblast for placental development. Mol. Cell. Biol. **25:**10979–10988.
24. **Ozer, A., L. C. Wu, and R. K. Bruick.** 2005. The candidate tumor suppressor ING4 represses activation of the hypoxia inducible factor (HIF). Proc. Natl. Acad. Sci. USA **102:**7481–7486.
25. **Peng, J., L. Zhang, L. Drysdale, and G. H. Fong.** 2000. The transcription factor EPAS-1/hypoxia-inducible factor 2α plays an important role in vascular remodeling. Proc. Natl. Acad. Sci. USA **97:**8386–8391.
26. **Percy, M. J., Q. Zhao, A. Flores, C. Harrison, T. R. Lappin, P. H. Maxwell, M. F. McMullin, and F. S. Lee.** 2006. From the cover: a family with erythrocytosis establishes a role for prolyl hydroxylase domain protein 2 in oxygen homeostasis. Proc. Natl. Acad. Sci. USA **103:**654–659.
27. **Roberts, A. W., L. Robb, S. Rakar, L. Hartley, L. Cluse, N. A. Nicola, D. Metcalf, D. J. Hilton, and W. S. Alexander.** 2001. Placental defects and embryonic lethality in mice lacking suppressor of cytokine signaling 3. Proc. Natl. Acad. Sci. USA **98:**9324–9329.
28. **Rossant, J., and J. C. Cross.** 2001. Placental development: lessons from mouse mutants. Nat. Rev. Genet. **2:**538–548.
29. **Ryan, H. E., J. Lo, and R. S. Johnson.** 1998. HIF-1 α is required for solid tumor formation and embryonic vascularization. EMBO J. **17:**3005–3015.
30. **Semenza, G. L.** 1998. Hypoxia-inducible factor 1: master regulator of O2 homeostasis. Curr. Opin. Genet. Dev. **8:**588–594.
31. **Semenza, G. L., M. K. Nejfelt, S. M. Chi, and S. E. Antonarakis.** 1991. Hypoxia-inducible nuclear factors bind to an enhancer element located 3′ to the human erythropoietin gene. Proc. Natl. Acad. Sci. USA **88:**5680–5684.
32. **Semenza, G. L., P. H. Roth, H. M. Fang, and G. L. Wang.** 1994. Transcriptional regulation of genes encoding glycolytic enzymes by hypoxia-inducible factor 1. J. Biol. Chem. **269:**23757–23763.
33. **Tian, H., R. E. Hammer, A. M. Matsumoto, D. W. Russell, and S. L. McKnight.** 1998. The hypoxia-responsive transcription factor EPAS1 is essential for catecholamine homeostasis and protection against heart failure during embryonic development. Genes Dev. **12:**3320–3324.
34. **To, K. K., and L. E. Huang.** 2005. Suppression of HIF-1α transcriptional activity by the HIF prolyl hydroxylase EGLN1. J. Biol. Chem.
35. **Wang, G. L., B. H. Jiang, E. A. Rue, and G. L. Semenza.** 1995. Hypoxia-inducible factor 1 is a basic-helix-loop-helix-PAS heterodimer regulated by cellular O2 tension. Proc. Natl. Acad. Sci. USA **92:**5510–5514.
36. **Wiesener, M. S., H. Turley, W. E. Allen, C. Willam, K. U. Eckardt, K. L. Talks, S. M. Wood, K. C. Gatter, A. L. Harris, C. W. Pugh, P. J. Ratcliffe, and P. H. Maxwell.** 1998. Induction of endothelial PAS domain protein-1 by hypoxia: characterization and comparison with hypoxia-inducible factor-1α. Blood **92:**2260–2268.
37. **Wilkinson, D. G., and M. A. Nieto.** 1993. Detection of messenger RNA by in situ hybridization to tissue sections and whole mounts. Methods Enzymol. **225:**361–373.
38. **Withington, S. L., A. N. Scott, D. N. Saunders, K. Lopes Floro, J. I. Preis, J. Michalicek, K. Maclean, D. B. Sparrow, J. P. Barbera, and S. L. Dunwoodie.** 2006. Loss of Cited2 affects trophoblast formation and vascularization of the mouse placenta. Dev. Biol. **294:**67–82.